Shape-recovering nanocellulose networks: Preparation, characterization and modeling

Ruiz, Maria F. Cortes; Brusentsev, Yury; Lindström, Stefan B.; Xu, Chunlin; Wågberg, Lars

Published in:
Carbohydrate Polymers

DOI:
10.1016/j.carbpol.2023.120950

Published: 01/09/2023

Document Version
Accepted author manuscript

Document License
CC BY-NC-ND

Journal Pre-proof

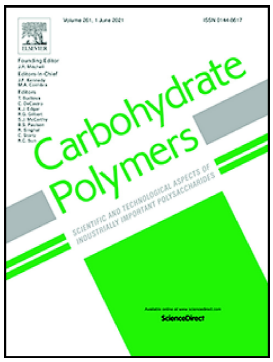

Shape-recovering nanocellulose networks: Preparation, characterization and modeling

Maria F. Cortes Ruiz, Yury Brusentsev, Stefan B. Lindström, Chunlin Xu, Lars Wågberg

PII: S0144-8617(23)00415-0

DOI: https://doi.org/10.1016/j.carbpol.2023.120950

Reference: CARP 120950

To appear in: *Carbohydrate Polymers*

Received date: 31 January 2023

Revised date: 20 March 2023

Accepted date: 22 April 2023

Please cite this article as: M.F. Cortes Ruiz, Y. Brusentsev, S.B. Lindström, et al., Shape-recovering nanocellulose networks: Preparation, characterization and modeling, *Carbohydrate Polymers* (2023), https://doi.org/10.1016/j.carbpol.2023.120950

Shape-recovering nanocellulose networks: Preparation, characterization and modeling

Maria F. Cortes Ruiz [a, b], Yury Brusentsev [c], Stefan B. Lindström [d], Chunlin Xu [c] and Lars Wågberg [a, b]*

[a] Fiber Technology Division, Fiber and Polymer Technology Department, KTH Royal Institute of Technology, 114 28 Stockholm, Sweden.

[b] Wallenberg Wood Science Center, Fiber and Polymer Technology Department, KTH Royal Institute of Technology, 114 28 Stockholm, Sweden

[c] Laboratory of Natural Materials Technology, Åbo Akademi University, 20500 Åbo Finland.

[d] FSCN Research Center, Mid Sweden University, 852 30 Sundsvall, Sweden.

*Correspondence to: wagberg@kth.se

ABSTRACT

Development of strong cellulose nanofibril (CNF) networks for advanced applications, such as in the biomedical field, is of high importance owing to the biocompatible nature and plant-based origin of cellulose nanofibrils. Nevertheless, lack of mechanical strength and complex synthesis methods hinder the application of these materials in areas where both toughness and manufacturing simplicity are required. In this work, we introduce a facile method for the synthesis of a low solid content (< 2 wt.%), covalently crosslinked CNF hydrogel where Poly (N-isopropylacrylamide) (NIPAM) chains are utilized as crosslinks between the nanofibrils. The resulting networks have the capability to fully recover the shape in which they were formed after various drying and rewetting cycles. Characterization of the hydrogel and its constitutive components was performed using X-ray scattering, rheological investigations and uniaxial testing in compression. Influence of covalent crosslinks was compared with networks crosslinked by the addition of $CaCl_2$. Among other things the results show that the mechanical properties of the hydrogels can be tuned by controlling the ionic strength of the surrounding medium. Finally, a mathematical model was developed based on the experimental results, which describes and

predicts to a decent degree the large-deformation, elastoplastic behavior, and fracture of these networks.

Keywords: Nanocellulose, networks, hydrogel, modelling, nanofibrils

Statements and Declarations:

Conflict of interest: The authors declare that they have no conflicts of interest

1 Introduction

Hydrogels, as a class of materials, are usually defined as three-dimensional networks composed of crosslinked, hydrophilic polymers capable of holding large amounts of water. They respond to different environmental stimuli (pH, temperature, ionic strength, etc.) in different ways depending on their composition. Due to these intrinsic properties, hydrogels are attractive materials in the fields of agriculture(Michalik & Wandzik, 2020; Rudzinski et al., 2012), biomedical engineering(Ashammakhi et al., 2019) and soft robotics(Lee, Song, & Sun, 2020; Sachyani Keneth, Kamyshny, Totaro, Beccai, & Magdassi, 2021; Shiblee, Ahmed, Kawakami, & Furukawa, 2019). Hydrogels can also be composed of cellulose nanofibrils (CNF) and these are particularly appealing for these applications due to their biodegradable and biocompatible nature. Due to their high anisotropy, stiffness and biodegradability, CNFs have been utilized as reinforcing elements in polymer matrices for composite materials (Ng, Sin, Bee, Tee, & Rahmat, 2017; Peng et al., 2020; Zinge & Kandasubramanian, 2020). Pure CNF hydrogels usually lack mechanical and chemical properties required (Heise et al., 2021), therefore, there have been several studies on chemical modifications and treatments of CNFs to fit different applications(Kang, Liu, & Huang, 2016). Recent developments in the design of polymeric hydrogels with tough and resilient properties(Creton, 2017) such as, double networks (Hagiwara, Putra, Kakugo, Furukawa, & Gong, 2009) or dual-crosslinked networks(Mayumi, Guo, Narita, Hui, & Creton, 2016), gives fundamental understanding of techniques used to delay the propagation of cracks and to further widen the property space of these materials. Such knowledge provides a route for further development of tougher CNF hydrogels for advanced applications.

In the biomedical engineering field, for instance, there has been an interesting development in the preparation of CNF-based hydrogels(Apelgren et al., 2021; Markstedt, Escalante, Toriz, & Gatenholm, 2017; X. Wang, Wang, &

Xu, 2020; Xu, Molino, et al., 2019). In these applications, CNF dispersions/inks have been used for 3D printing of tissue scaffolds where the rheological properties of the dispersions and the structural similarity of CNF hydrogels to extracellular matrices (ECM)(Apelgren et al., 2021; Nemir & West, 2010; X. Wang et al., 2020) have been exploited. Current cellulose-based bioink formulations often use second biopolymer networks, such as collagen,(Xu, Molino, et al., 2019) alginate(Markstedt et al., 2015) or modified polysaccharides,(Markstedt et al., 2017; Xu, Zhang, et al., 2019) to enable crosslinking of the formed hydrogels and to add structural stability. These formulations can be rapidly crosslinked during or after printing using direct chemical crosslinking(Markstedt et al., 2017), indirect crosslinking via UV-irradiation(Q. Wang, Backman, Nuopponen, Xu, & Wang, 2021), physical crosslinking using an addition of multivalent salts(Markstedt et al., 2015) or pure physical entanglements depending on their overall composition.

A different approach, to simplify the hydrogel preparation procedure, and to add desirable material properties to the hydrogels, could be to modify the surface of the CNFs, or even the fibers before CNF preparation, to enable direct crosslinking of the fibrils. Some well-known chemical modifications of cellulose, including ring opening reactions (such as periodate oxidation), surface adsorption, modification of the hydroxyl groups and polymer grafting could be suitable for the preparation of CNF hydrogels with tailored properties(Rol, Belgacem, Gandini, & Bras, 2019). The introduction of electrostatic charges by modification of hydroxyl groups allows for physical crosslinking of CNFs by addition of multivalent salts.(Benselfelt, Nordenström, Hamedi, & Wågberg, 2019; Benselfelt, Nordenström, Lindström, & Wågberg, 2019) Such modifications can be achieved by TEMPO oxidation(Isogai, Saito, & Fukuzumi, 2011; Saito et al., 2009), carboxymethylation(Wågberg et al., 2008) and cationization(Aulin, Johansson, Wågberg, & Lindström, 2010) just to mention a few of the well-known modification techniques. An alternative would be to introduce reactive groups onto the CNFs that would allow for the formation of more permanent crosslinks in the CNF hydrogel(Kang et al., 2016). As an example of this, Kelly and coworkers introduced methacrylate groups on cellulose fibers by esterification under alkaline aqueous conditions(Kelly, Cheng, Gardner, & Gramlich, 2021). Following this step, a polymer grafting was achieved through a facile radical polymerization. By utilizing a similar modification, CNFs can be covalently crosslinked directly with a flexible polymer. We suggest that such crosslinks would prevent any change in the fibril/fibril contacts, i.e. sliding between the fibrils, during water removal providing the base for a shape-recovery of the material upon rewetting. In turn, this will also result in a material with better physical and mechanical properties compared to ionically crosslinked networks.

In this work, a procedure for the preparation of elastic, covalently crosslinked (C-x) CNF-based hydrogels is described together with an extensive characterization of their chemical and mechanical properties under different conditions. Based on these results, a theoretical model was developed for the large-deformation, nonlinear-elastic properties and fracture of the differently-prepared hydrogels. The fibers used for the preparation of the CNF were surface modified to contain anionic charges as well as methacrylate groups, providing excellent colloidal properties to the CNF and the capability to be directly crosslinked (Figure 1a and b). Furthermore, by utilizing poly (N-Isopropyl Acrylamide) as a linker, it was shown possible to control swelling, deswelling and to create rubber-like properties of the prepared hydrogels. The results show, among other things, a remarkable shape recovery of the covalently-crosslinked network. As a comparison, networks crosslinked only by ionic (I-x) (addition of $CaCl_2$) crosslinking or by a combination of both ionic and covalent means (D-x) (addition of $CaCl_2$ after polymerization) were prepared with the same type of fibrils and characterized in the same way (Figure 1c). The theoretical model developed based on the experimental data describes the network mechanics, predicts the macroscopic behavior of the hydrogels, and enables further development of these outstanding materials.

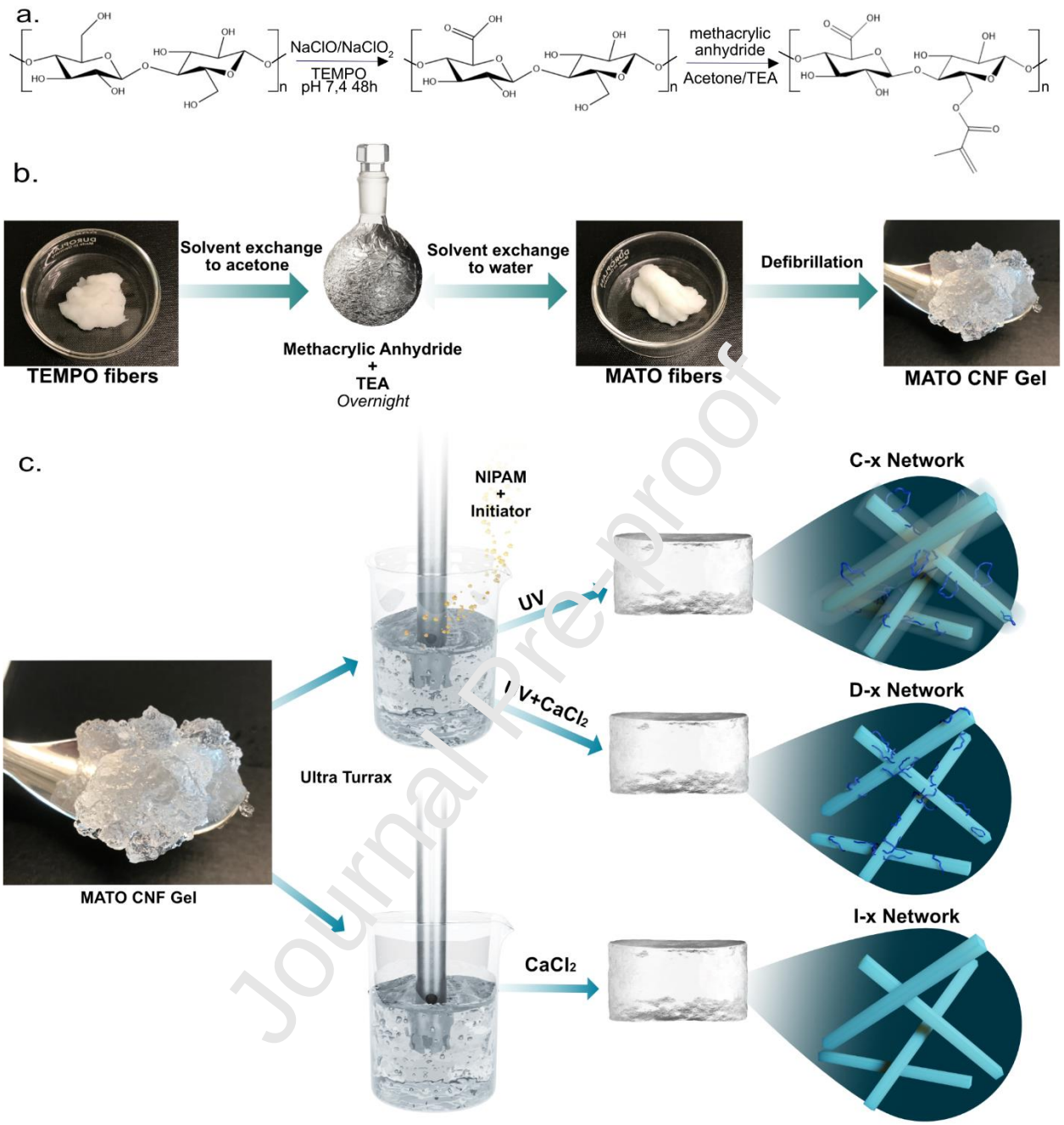

Fig. 1 *(a.) Proposed chemical mechanisms for the cellulose modification (b.) Schematic of the chemical modification procedure (c.) Synthesis and proposed structures of hydrogel networks with the crosslinking methods studied*

2 Experimental Section

2.1 Materials

Never-dried dissolving pulp with a cellulose content of 98% was kindly provided by Aditya Birla, Domsjö Fabriker AB, Örnsköldsvik, Sweden. (2,2,6,6-tetramethylpiperidin-1-yl) oxidanyl (TEMPO) (purity of 98%), sodium chlorite (80% purity), Methacrylic anhydride (94% purity), triethylamine (99.5% purity), calcium chloride (97% purity), N-Isopropyl acrylamide (97% purity) and 2-Hydroxy-4′-(2-hydroxyethoxy)-2-methylpropiophenone (Irgacure 2959) (98% purity) were purchased from Sigma-Aldrich. Sodium hypo chlorite (14% Cl2), acetone, potassium phosphate and sodium hydroxide were purchased from VWR. All chemicals were used without further purification.

2.2 Synthesis of Methacrylated TEMPO oxidized nanofibrils (MATO)

The never-dried dissolving pulp (15g dry weight) was TEMPO oxidized at 60 °C in neutral conditions following a previously described procedure,[22] and allowed to react for 48 hours to reach a carboxylic acid content of 0.920 mmol/g. After TEMPO oxidation, the pulp was rinsed with MilliQ water until the filtrate reached a conductivity of less than 5µS. The TEMPO-oxidized pulp was then dispersed in MilliQ water with 0.001M of $NaHCO_3$ and raised to pH 9 using 0.1M NaOH before being washed again with MilliQ water until the filtrate showed a conductivity below 5µS. Ten grams (dry weight) of TEMPO-oxidized pulp were solvent exchanged three times with acetone (3 x 100 mL) with help of vacuum filtration to remove all the trapped water in the fibers. After effective water removal, the fibers were dispersed in 100 mL acetone using a magnetic stirrer. To this mixture were added 10 mL of triethylamine (~140 mmol) followed by dropwise addition of 9 mL of methacrylic anhydride (~60 mmol). The resulting mixture was transparent and the fibers had a white color and a cloud-like appearance. The vessel was sealed, wrapped in aluminum foil, and allowed to react on top of a GFL3015 Orbital Shaker table at moderate speed overnight. The fibers were subsequently rinsed twice with 50mL of acetone and then with 15 L of MilliQ water using a vacuum filtration system until the conductivity of the water was below 5µS.

The MA TEMPO pulp (~9g of solid content) was dispersed in 750 mL of MilliQ water. The resulting fiber dispersion was mechanically defibrillated at a concentration of ~12g/L using a high-pressure microfluidizer (Microfluidizer M-110EH, Microfluidics Corp.). The fiber dispersion passed twice through a 400µm/200µm chamber configuration and 3 more times through a 200µm/100µm chambers configuration.

2.3 Hydrogels synthesis

After homogenization, the dispersion was diluted to the desired concentrations. The dispersions intended for C-x networks were mixed with N-Isopropyl acrylamide (final concentration of 1wt.% unless stated otherwise) and 2-Hydroxy-4′-(2-hydroxyethoxy)-2-methylpropiophenone (Irgacure 2959) (final concentration of 0.2 wt.%). Dispersions intended for I-x networks were naturally kept pristine. All dispersions were homogenized for 5 min at 9000 rpm using an ultra turrax. The neat cellulose dispersion intended for I-x samples was also dispersed with ultra turrax at the same frequency and time to ensure all dispersions had the same mechanical treatment. The bubbles in the dispersions were removed by centrifuging at 4000 rpm for 15 min or until all the bubbles disappeared.

I-x networks were prepared by pouring 1.2 g of dispersion into cylindrical PDMS molds of 25 mm in diameter and 2 mm in height. A piece of prewetted hydrophilic membrane with a pore size of 0.65µm was placed on top of the dispersion making sure no bubbles are formed in the process. An aliquot of 0.2 M $CaCl_2$ was used to a final COO^- to M^{2+} ratio of approximately 1:20. A spatula was used to spread the liquid evenly on top of the membrane. A plastic centrifuge cap was placed as a cover to hinder dehydration. The entire mold was kept inside a petri dish with a few milliliters of water around the mold to keep a high relative humidity inside the chamber. The electrolyte solution was allowed to diffuse for at least 2 hours prior to measurement.

C-x networks for rheological studies were made by pipetting the NIPAM/CNF mixture and crosslinking it directly on the rheometer using a UV fixture (Figure 2a). For the D-x samples, C-x samples were lifted from the rheometer right after polymerization using a spatula and dipped in a petri dish with an electrolyte solution of the desired concentration (to a final charge ratio of 1:20). Samples remained in the electrolyte solution at least 2 hours prior to measurement. For compression and reswelling measurements, C-x networks were synthetized by crosslinking the formulation inside of a 5mL polypropylene syringe (8mm inner diameter) under an 8W mercury lamp at a wavelength of 365nm, and 10 cm distance from the source for at least 15 min. The samples were removed, sliced in cylindrical pieces and placed in MilliQ water for 24 hours prior to the measurement. The water was changed 3 times during those 24 hours to ensure effective removal of unbonded polymer. D-x networks were formed by placing C-x specimens in salt solution for at least 4 hours prior to measurements.

2.4 Chemical Characterization

2.4.1 Determination of degree of substitution

After modification, a small sample of fibers (roughly 1 g dried weight) was acidified to pH 3.6 using 0.1M acrylic acid to remove sodium ions. The sample was filtered and then neutralized with 0.1M triethylamine. The sample was finally rinsed with MilliQ water, filtered and freeze dried. A small amount of the freeze-dried sample was dissolved using an ionic liquid (consisting of DMSO-d6 and 25% of n-$Bu_4N^+OAc^-$) and analyzed by ^{1}H-NMR spectroscopy using diffusion filtration pulse program (see Supp. Info. I for details) to enhance sensitivity. The percentage of the methacrylic groups was found to be around 7% of the monosaccharide units.

2.4.2 Determination of polymer chain length in between fibrils

Extraction of the polymer links in the hydrogel was performed by alkaline hydrolysis treatment followed by purification and analysis. In a centrifuge tube, a 20g formulation containing 1wt.% CNF, 1wt.% PNIPAM and 0.2 wt. % initiator (Irgacure 2959) was polymerized using UV light irradiation of 365nm wavelength for at least an hour. The resulting gel was sliced into smaller pieces and submerged in ice cold MilliQ water to diffuse out all of the un-crosslinked polymer. The water was collected in a round flask and replaced three times during 24 hours. The water collected with the unbounded polymer was freeze dried and weighed. The dried remains were analyzed with NMR and HP-SEC.

The washed hydrogel pieces were submitted to alkaline hydrolysis by placing them in a 25mL solution of 0.5 M NaOH and 100µL of 1M $NaHCO_3$. The reaction is allowed to proceed for 14 days under vigorous magnetic stirring. At this time, the gel has lost most of its shape and it is broken in even smaller pieces. Concentrated HCl was carefully added to the mixture to decrease its pH to 2 and kept at this pH for at least 24 hours. The acid mixture was dialyzed against MilliQ water in a dialysis tube with a pore size of around 3.5kDa for 4 days. The dialyzed mixture was filtered with 0.65 µm pore membrane and the residue on the filter was rinsed further with 200mL of ice cold MilliQ water. The filtrate was freeze dried, weighed and analyzed using HP-SEC and NMR.

2.5 WAXs and SAXs investigations

Changes in fibrillar and network structure upon drying and reswelling were studied using wide-angle X-ray scattering (WAXs) and small-angle X-ray scattering using a SAXSpoint 2.0 system (CuKα λ=1.5418 Å, Anton Paar., Austria) with an Eiger R1 M detector (Dectris Ltd., Switzerland) of pixel size 75 x 75 µm and a beam size of

≈500 μm. For the WAXs investigations the sample to detector distance (SSD) was about 111mm for both air-dried and CPD dried gels. For SAXS measurements the SSD of 563 mm.

2.6 Rheological Characterization

The rheological assessment was performed in a DHR-2 rheometer (TA Instruments, New Castle, DE, USA) equipped with a Peltier system for temperature control and a solvent trap to hinder evaporation. To limit the effect of slippage at the boundary, the plate-plate geometries used were roughened onsite with help of sandpaper with grit of 60, plasma treated for 2 minutes and coated with a poly allyl imine hydrochloride (PAH) solution at pH 3 for at least 15 min. The surfaces were rinsed with MilliQ water and dried at room conditions with a nitrogen gas before the measurements. The acrylic crystal used during in situ UV curing was also chemically treated with plasma treatment and PAH coating. The bottom surface of the Peltier plate system was covered with a 1 mm thick aluminum surface which was roughened and chemically treated onsite the same way as the aluminum, disposable geometries.

The polymerization of the gels was carried out in situ using a UV fixture and a 20 mm diameter disposable geometry with a 1mm gap. The concentration of the gels studied was between 0.3wt.% to 1wt.% with a constant monomer concentration (NIPAM) of 1wt.% The UV fixture used a narrow wavelength (365 nm) LED with a maximum intensity of 150 mW/cm^2 at the surface of the crystal.

The electrolyte-locked samples were made on CNF concentrations from 0.15% to 1 wt. %. They were removed from the molds, and then placed on the rheometer plate. This method prevents any damage to the network during transfer. For these samples, the roughened and chemically-treated 25 mm plate-plate geometry described above was used to improve contact to the sample with a gap of 2 mm.

The polymerization of UV samples was followed during a 5 minutes time sweep at 10 rad/s and 1% strain where the UV irradiation began after 50 seconds with an approximate intensity of 15mW/cm^2 at the surface of the hydrogel.

All samples were allowed to equilibrate for at least 2 minutes before measurement. Strain-amplitude sweeps for all samples were made between 0.1 and 500% strain on a logarithmic sweep at a frequency of 10 rad/s. Repeated creep tests were performed in all samples with an initial stress of 5 Pa which, based on the amplitude sweep data of all three type of networks, it appeared to be in the LVR for all of them. The samples were submitted to 1 min creep and

2 min recovery cycles in which the stress applied was doubled after each cycle. The test last until the network showed either catastrophic failure or slipped out of the geometry. The deformation and recovery during each cycle was used to describe the elastic and viscous nature of each network. In all cases, failure was observed at stresses beyond the LVR.

2.7 Mechanical Characterization

The uniaxial-compression mechanical characterization of the hydrogels was performed in a single column Instron 5944 equipped with a 500N load cell. All samples measured were made with an initial CNF concentration of 1wt.%. The electrolyte-locked samples were made in the same way as the samples for the rheometer, but in this case samples with 8mm diameter were punched out of gels formed in the mold. The samples were stored in the same electrolyte solution used for "crosslinking" until they were measured. The C-x networks were crosslinked inside a 5mL syringe (1cm inner diameter). The C-x and D-x networks were kept in MilliQ water and electrolyte solution respectively for 24 hours prior to measurement. The compression rate used for all samples was 0.5 mm/s and the maximum strain for the cyclic tests was 25%. A small piece of P600 grit sand paper was placed at the bottom plate to prevent the samples from slipping out of the plates.

3 Results and Discussion

3.1 Chemical Characterization of the fibrillar networks

The mechanical properties of CNF networks are highly dependent on the chemical and mechanical treatment used to modify and liberate the individual fibrils, and special attention was therefore devoted to characterization of the chemical and physical properties of the fibrils used. The total carboxylic acid content on the CNF was 0.920 mmol/g (DS 0.15) and the degree of substitution of methacrylic acid groups, calculated from Nuclear Magnetic Resonance (NMR) experiment, was around 7% (0.42 mmol/g) of the totally amount of monosaccharide units. The average thickness and length of the fibrils measured using Atomic Force Microscopy (AFM) was around 2.46 (±0.74) nm and 432.5 (±257) nm respectively with an aspect ratio of approximately 176. The dimensions of these CNFs are on average rather short compared to those reported in literature.(Foster et al., 2018; Nechyporchuk, Belgacem, & Bras, 2016) To clarify the effect of the chemical and physical treatment on the crystallinity of the fibrils, Wide Angle X-ray Scattering (WAXs) was utilized. From these investigations, it was clear that the methacrylation reaction had little effect on the crystallinity of the TEMPO-oxidized fibers. However, it was also demonstrated that the process of

mechanical defibrillation into CNFs induced a significant loss in crystallinity compared to the chemically modified fibers. Details regarding this characterization are given in Supporting Information I.

C-x networks were formed by combining the MATO CNF dispersion with NIPAM monomer and initiator (Irgacure-2959) followed by a UV-initiated polymerization. The polymerization reaction was followed using photo-rheology where the dynamic storage modulus of the formulation was monitored before and after UV irradiation (Figure 2a and b). For all investigated CNF concentrations, the storage modulus (*G*') reaches a plateau within the first 2 minutes of irradiation. The increment in *G*' was proportional to the CNF concentration, which is reasonable given the higher availability of methacrylic sites and the shorter distance between fibrils at the higher concentrations.

3.2 Reswelling capacity and shape recovery

In terms of stability in water, all networks tested were shown to maintain their structure in water for several weeks after crosslinking regardless of crosslinking method. When allowed to equilibrate in MilliQ water for 24 hours, C-x networks (at 1wt.% MATO CNF and 1wt. % monomer) swelled around 67% from their initial volume while I-x networks, at the same CNF content, retained their initial shape and volume. The additional swelling of C-x networks in water is a result of the build-up of a large internal osmotic pressure in the network dominated by the surface charges of the fibrils but also, to a minor extent, to the presence of non-bonded polymer remaining in the network. After drying at ambient conditions and re-submerging in water, C-x networks (at 1 wt.% MATO CNF and 1 wt.% monomer) reswelled up to 119% of their initial weight compared to I-x and D-x networks, which did not reswell regardless of the CNF content. This latter effect is also in accordance with earlier investigations (Benselfelt, Nordenström, Lindström, et al., 2019). The reswelling capacity of the C-x networks was tested through 3 drying/rewetting cycles at ambient conditions and it was observed that the maximum reswelling was achieved during the first cycle and decreased slightly after every cycle (Figure 2c). This indicates that the C-x network is strong enough to withstand the capillary forces during drying and that there is a mechanism preventing hornification of the fibrils(Laivins & Scallan, 1993) and permanent collapse of the structure. Nevertheless, after every drying cycle, the network seems to yield to some extent.

Due to the versatility of the method, it was possible to create hydrogels with a variety of shapes by adding the formulation into silicon molds and placing the molds under the UV light. It was also clear, that if allowed to dry at

ambient conditions and then to reswell in deionized water, the hydrogel hydrated back into the shape it was originally crosslinked (Figure 2d to 2f). The effect of drying and reswelling on the structure of the C-x network was assessed by both SAXS and WAXS investigations of the hydrogel in the never-dried state, dried under ambient conditions and in the rehydrated state. As a comparison, a MATO CNF dispersion was used to clarify the role of the polymer links. The samples were solvent exchanged into absolute ethanol and dried in this "swollen state" by using Critical Point Drying (CPD) to decrease the water signal during measurement. The results from the WAXS investigations showed that the signals from the never-dried and the reswollen hydrogels were basically identical, indicating that the distance between the crystal planes of the CNFs was not affected by the drying/rewetting cycle (Figure 2g).

For the collapsed, air-dried network, there is an extra signal at lower scattering vectors (q values) which cannot be ascribed to the cellulose. This signal can most probably be ascribed to an ordering of the PNIPAM chains onto the surface of the fibrils upon drying at room temperature. A more detailed study of the conformation of PNIPAM chains in solution can be found elsewhere (Yanase, Buchner, & Sato, 2018). The SAXS investigations showed a significant difference between the never-dried and the reswollen networks (Figure 2h). The maximum signals in the Kratky plots indicate a shift in the average pore size of the networks from 34 nm (q value of 0.18) to 20.4 nm (q value of 0.31) after the drying and reswelling cycle, which is in accordance to the decrease in swelling capacity. These investigations also showed the presence of a porous structure in the ambient-dried network with an average pore size of 10 nm (q value of 0.63) (Figure 2i). This porosity was not observed when a dispersion of the same MATO CNFs was allowed to dry under the same conditions, suggesting that upon drying, the C-x network preserves its overall structure with, naturally, shorter distances between the fibrils.

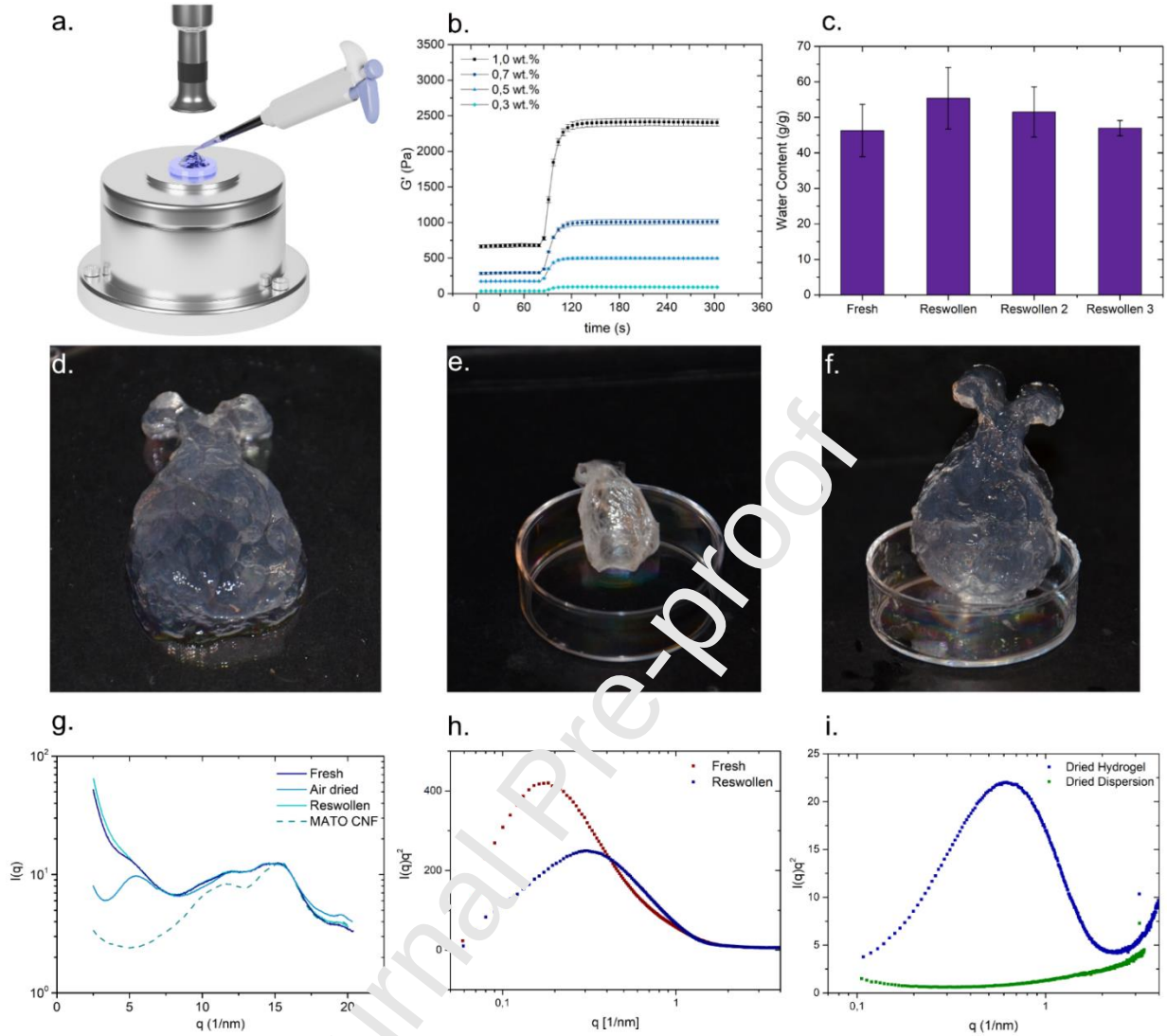

Fig. 2 *(a.) Artistic schematic of the photo-rheology experiments (b.) Development of storage modulus G' during photo-crosslinking at different MATO CNF concentrations (c.) Reswelling capacity of C-x networks (d-f) C-x network in the shape of a pineapple freshly made, air dried and reswollen in water (g.) Effect of drying/reswelling cycles observed with WAXS and (h. and i.) Kratky plots from the SAXS measurements*

In the C-x hydrogels the CNFs are hold together due to both covalent linkages between the PNIPAM and the CNFs and to possible physical adsorption of the PNIPAM to the cellulose. The physical interactions between the PNIPAM polymer chains and MATO CNF were analyzed through adsorption measurements using Quartz Crystal Microbalance with Dissipation (QCM-D) (See Supp. Info. I for details). These measurements showed a clear adsorption of PNIPAM onto MATO CNF, which indicates, that the polymer chains, have a preferred adsorption onto cellulose. To investigate further the characteristics of the polymer crosslinks, the links in the CNF network

were cleaved, the polymers extracted and analyzed for dimensions and chemical identity utilizing High Performance Size Exclusion Chromatography (HP-SEC) and NMR respectively. Due to the chemical properties of the Poly-NIPAM/methacrylate chains and their interactions with cellulose, the recovery of the cleaved chains was very limited with a yield of only 15% of the expected total polymer in the gel. This could be explained by the high affinity of the PNIPAM polymer to cellulose fibrils which lead to low yield of extraction. The average molecular weight of the extracted polymer was 188 kDa with a polydispersity of around 2.3. Comparing the chain-length distribution of the extracted polymer with the theoretical distance between methacrylate groups, it is evident that the shortest polymer chain extracted is significantly larger than the calculated distance between methacrylate groups (Details of this calculation are found in Supp. Info. I). This theoretical estimation indicates that when the hydrogels are dried, the grafted polymer chains will collapse onto the fibril surface, effectively coating the surface and preventing direct interaction between cellulose. In this way, the hornification between cellulose fibrils can most likely be avoided, which indeed contributes to the excellent reswelling behavior of the networks. Reswelling of C-x networks was only observed in networks with CNF concentration above 1 wt.% suggesting that there is an induced, built-in stress, between fibrils in the network upon water removal which might contribute positively to the reswelling behavior when this stress is released by the added water. As a comparison, I-x and D-x networks did not show any reswelling properties regardless of concentration. A structural comparison between C-x and I-x networks was also performed using SEM imaging (See Supp. Info. I). It was observed that the networks displayed a very similar network topography although it is clear that I-x networks have a more compact structure.

3.3 Rheological Characterization

In order to compare the rheological properties of the in-situ UV-crosslinked C-x networks with the I-x networks, it was necessary to prepare an I-x locked network in a non-disturbed state. Therefore, samples of I-x were prepared in specially-designed silicon molds at different solids concentrations with the exact geometry needed for the study, and then transferred to the rheometer (Figure 3a). As shown in Figure 3b, the concentration dependence of G' for both the non-crosslinked dispersion and the C-x network follow a power law relation with similar order but with different pre-factors, manifested as parallel displacement of the curves. I-x networks and D-x networks also showed similar relations (Figure 3c) with lower slopes. This type of logarithmic relationship, i.e. $G'=k\phi^n$, with ϕ representing the volume fraction of cellulose, is commonly found in fibrillar networks and has also been observed for CNF

networks(Saito, Uematsu, Kimura, Enomae, & Isogai, 2011; Tatsumi, Inaba, & Matsumoto, 2008; Tatsumi, Ishioka, & Matsumoto, 2002). In this mathematical relation, the exponent *n* is used to characterize the structure of the network and mode of deformation of the fibrils, while the constant *k* is used to characterize the properties of the individual fibrils. In the case of CNF networks, both parameters are highly dependent on the characteristics of the fibrils and their manufacturing process. The values reported in the literature vary due to the differences in aspect ratio, surface charge and flexibility of the individual fibrils, as well as the method used to form the fibrillar networks (Tatsumi et al., 2008). In 2008, R.J. Hill proposed a model that considers the intrinsic properties of the constituent fibrils and their interactions (Hill, 2008). By utilizing the data from Päkkö and co-workers(Pääkkö et al., 2007), Hill developed a model covering different volume fraction regimes of CNF. In the dilute regime the slope (*n*) appeared to be 3.7 and the constant pre-factor (*k*) was 2.25 Pa. Nevertheless, this model does not consider crosslinked fibrillar networks with neither permanent nor dynamic bonds. The fibrils utilized in the present work have the same origin, were manufactured in the same way and the only difference between the networks is the crosslinking method. Therefore, the parameters *n* and *k* from the initial power law relationship will be utilized to compare the effect between the crosslinking types studied.

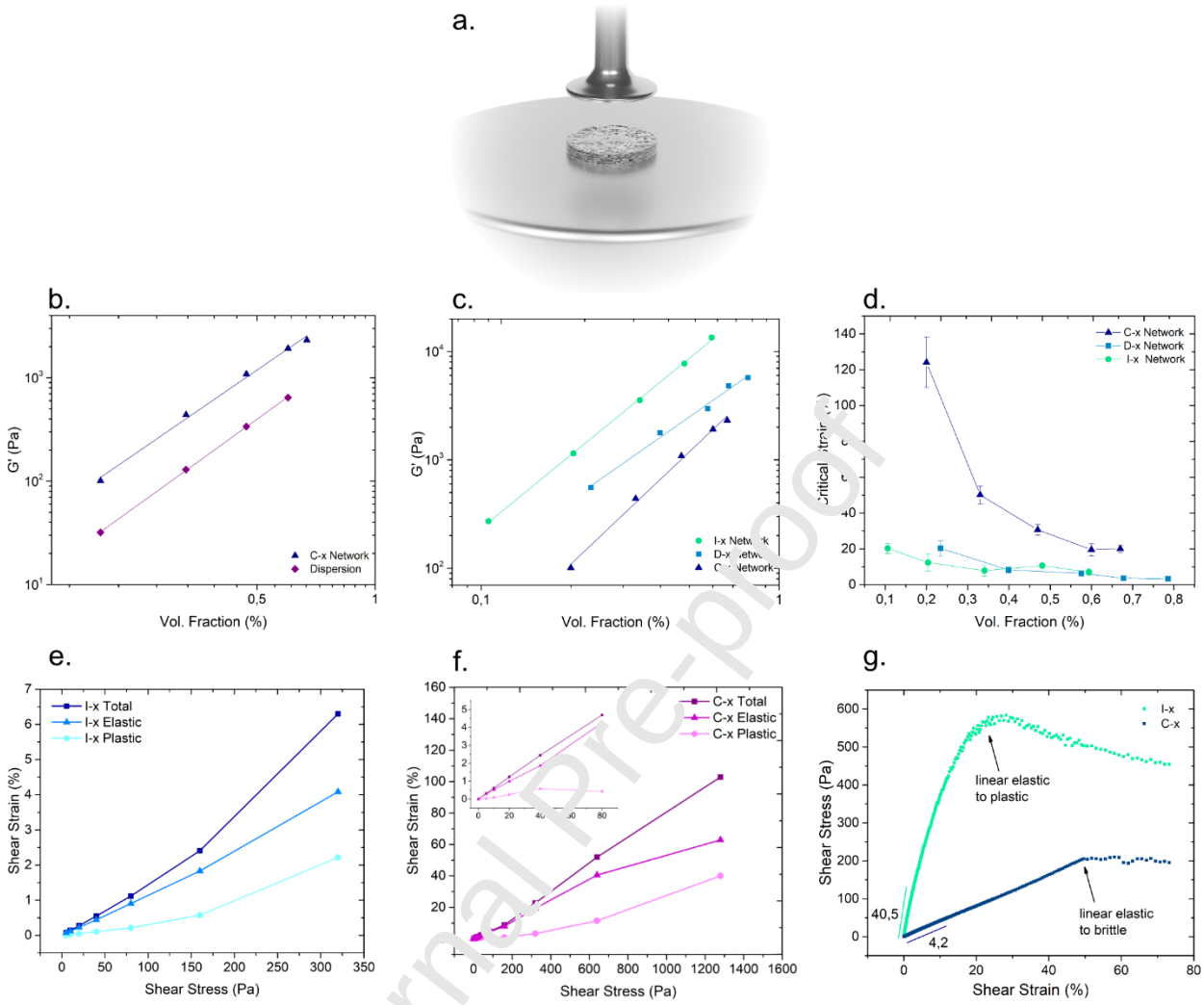

Fig. 3*(a.) Artistic schematic of a pre-formed hydrogel prior to testing (b.) Comparison of G' as a function of cellulose vol. fraction before and after polymerization (c.) Comparison of G' and (d.) critical strain of the crosslinking methods studied as a function of vol. fraction. Total, plastic and elastic deformation from creep and recovery measurements for (e.) I-x and (f.) C-x at 0.9 wt.% CNF with a zoom-in at lower shear strains (g.) Deformation transitions of I-x and C-x to either plastic or brittle during strain ramp measurement at 0.7% CNF. Figures 3e to 3g are representative of the behavior of the networks at the CNF concentration range studied (0.15 wt.% to 0.9 wt.%)*

Table 1 summarizes parameters *n* and *k* for the networks studied. The structure of the hydrogels was compared using the differences in the scaling (*n*) of *G*' as a function of volume fraction of cellulose. It was observed that for the C-x network and the un-crosslinked dispersion *G*' scales with *n* equal to 2.6 and 2.7, respectively. This suggest that the initial network structure of the fibrils in dispersion was not significantly disturbed by the creation of polymer crosslinks. On the other hand, I-x and D-x networks had a scaling factor *n* closer to 2. This reduction in scaling

factor reflects an apparent change in the structure of the network induced by the addition of the electrolyte. Figure 3c displays the effect of these structural differences on the modulus of the networks as a function of volume fraction.

Table 1 Network parameters, achieved by fitting the data in figure 3 to the $G'=k\phi^n$ relationship

	k[Pa]	*n*	R^2
Dispersion	3.42	2.74	0.998
C-x Networks	3.86	2.61	0.994
I-x Networks	4.61	2.24	0.999
D-x Networks	3,98	1.93	0.989

When the CNF dispersion is covalently crosslinked by UV polymerization in the presence of NIPAM, the surface charges of the fibrils remain intact and cause a significant repulsion between fibrils. Therefore, the only physical contact between fibrils are those created by the polymer crosslinks. When $CaCl_2$ is added to the dispersion, the repulsive forces between fibrils diminish, and the fibrils are allowed to move closer to each other inducing both ionic crosslinks and physical entanglement. This diffusion induced rearrangement has been observed to cause alignment, and even anisotropy to some degree, in similar systems such as TEMPO CNF(Saito et al., 2011) and polyelectrolytes in dispersion.(Qiao, Du, Gong, Wu, & Zheng, 2019)

Comparison between the *k* values of the networks could be used to assess the changes in intrinsic properties of the individual fibrils due to crosslinking method. It was observed that I-x and D-x networks had a higher *k* value compared to C-x network and the un-crosslinked dispersion. This change in *k* with the addition of $CaCl_2$ might be an indication of a change in apparent aspect ratio of the fibrils after the charges are screened, causing an increased number of contacts between fibrils. Due to the presence of the electrostatic double layer around the charged fibrils (C-x and un-crosslinked dispersion), there is a natural repulsion between the fibrils due to the electro-osmotic interactions caused by these counterion clouds. This is expressed as an increased apparent diameter as compared to fibrils whose charges have been screened with salt (I-x and D-x networks). As the ionic strength is increased, the extension of the double layer will naturally decrease. The particles will have both a larger apparent aspect ratio and lower repulsive interactions allowing for a much larger number of contacts between the fibrils, which leads to an increase in *G*'. Additionally, as Benselfelt and coworkers previously described, the high surface charge density of the TEMPO-oxidized fibrils will actually lead to an attractive interaction between the fibrils when divalent ions are added (Benselfelt, Nordenström, Hamedi, et al., 2019). The friction forces, a consequence of physical

entanglements, and the attractive forces, caused by the Ca^{2+} ions in I-x networks, in combination with van der Waals interactions make the hydrogel stiffer, although the links are dynamic in nature. Thus, the fibrils of this system are able to slide against each other and deform earlier than in the C-x networks where the crosslinks are permanent and dependent on the strength of the polymer links.

The limiting critical strain of the Linear Viscoelastic Regime (LVR) and the onset of plastic deformations of the network was defined in this work as the point at which the pseudo-equilibrium *G'* (Storage modulus in the plateau region) was decreased by 10% in the amplitude- sweep oscillatory measurements. During these measurements (Figure 3d), I-x networks showed the lowest critical strain of the studied networks, indicating that these networks begin to deform at lower strains than the other systems regardless of CNF concentration. On the other hand, C-x networks had the largest critical strain, indicating a much more elastic network. After addition of $CaCl_2$ (during the synthesis of D-x networks), the dynamic moduli of the C-x network increased considerably at the same time as the critical strain was decreased. This reduction of elasticity indicates that the network interactions induced by the addition of salt, considerably increased friction and attractive forces due to the divalent cations. These effects are prevalent in the rheological behavior of the network for all concentrations studied.

The viscous and elastic nature of the hydrogels were further studied through repeated creep and recovery measurements at increasing shear stresses until the samples experienced catastrophic failure. It was observed that the C-x networks were capable of withstanding large shear stresses and their deformation was mostly elastic, while I-x networks were relatively stiffer (Figures 3e and 3f). Furthermore, C-x hydrogels were capable of withholding 4 times more shear stress and up to 10 times larger shear strains than the I-x hydrogels. The behavior of the C-x networks seems to be almost completely elastic up to stresses of around 160 Pa (Figure 3f) and it is most likely due to the elasticity of the polymeric crosslinks between the fibrils. The deformation of the networks was analyzed further using strain ramp measurements (Figure 3g). As observed from the previous measurement, C-x networks experienced a mostly linear elastic deformation ending in a brittle breakage of the polymer links. In the case of I-x, the network undergoes a transition from linear elastic to plastic deformation. This finding supports the idea that the fibrils in the I-x networks slide against each other and form new contacts along the way, while the integrity of the C-x networks is mandated by the elasticity of its polymer links. It is also worth noticing that the slope of the strain-

stress curve for I-x networks is about 10 times that of the C-x networks. This could be ascribed to the larger number of contacts between the fibrils in the I-x network compared to the C-x network as mentioned before.

3.4 Mechanical Characterization in Compression

The large-deformations behavior of the hydrogel was also studied using static and cyclic compressive loading. For the C-x networks, the strength was highly dependent on the degree of swelling and it was naturally observed that the degree of swelling was dependent of the ionic strength of the surrounding solution and therefore, it could be controlled. As mentioned earlier, the charges of the TEMPO-oxidized fibrils will contain a substantial amount of counterions, and in these polyelectrolyte gels this will create a large osmotic swelling pressure due to the imbalance between the concentration of ions inside and outside the gel. In simple terms, this means that in the case of MilliQ water, water flows freely into the network to dilute the high concentration of ions in the gel. The network in this case expands as much as possible to allow for this dilution. This expansion is likely due to the stretching of the polymer bridges between the fibrils which allow the overall network to hold its shape while increasing in volume (figure 4). In the case of aqueous media with a higher ionic strength compared to the ionic strength inside the network, the water inside the network will flow out instead and the network will shrink in size. Thus, the degree of expansion or collapse is dependent on the magnitude of the difference in osmotic pressure between the network and the medium.

When the swelling is maximized by allowing it to swell in MilliQ water, the network shows stiff and brittle behavior (Figures 5a and 5b). This indicates that fully swollen networks are already pre-stressed (polymer crosslinks fully stretched) and that the osmotic pressure inside of these gels should be superimposed onto the normal stress applied to the hydrogel during loading.

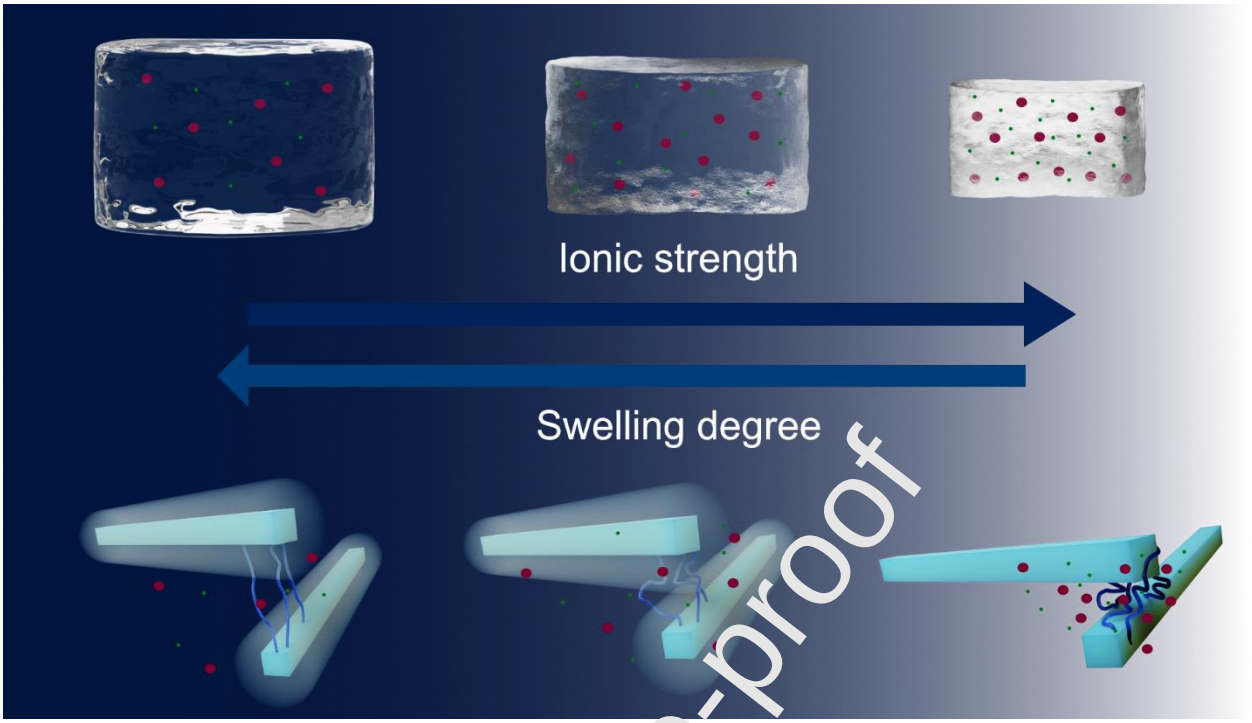

Fig. 4. *Visual representation of the swelling mechanism for the covalently crosslinked gels. Red and green dots represent ions within the gel. High ionic strength of the medium induces a shrinkage of the network while low ionic strength causes an expansion of the network and a stretch of the polymer crosslinks.*

On the other hand, in the case of D-x networks where the swelling is minimized by the screening of surface charges, one should also consider the effect of the divalent salt used in this work. As it was mentioned earlier, divalent salts such as $CaCl_2$ not only reduce the expansion of the double layer but will also induce an attractive interaction between the negatively charged fibrils, creating physical entanglement and ionic crosslinks (Benselfelt, Nordenström, Hamedi, et al., 2019; Bratko, Jönsson, & Wennerström, 1986). As the networks are compressed, some bonds are irreversibly broken while new ionic bonds are formed. Additionally, the polymer links would be in a more coiled state and would be able to withhold larger strains. These molecular interactions would help dissipate energy during deformation and delay the propagation of cracks. Although these hydrogels would suffer irreversible deformation, they would display a larger stress and strain at break. As a comparison, I-x networks are softer and display a densification behavior at larger strains.

The degree of deformation and its mechanism was studied further during cyclic deformation. A 25% maximum strain was selected for this study since this region was available for all crosslinking methods. It must be recalled that

due to the swelling pressure within the networks, the stresses are considerably different for the different networks, at these deformations. For the fully-swollen C-x networks, the loss of strength was irreversible after every cycle (Figure 5c) indicating significant loss of covalent bonds in the network during deformation. Nevertheless, during the second and third cycle, a more elastic behavior (smaller hysteresis) was observed. For D-x networks, the loss of strength appeared to be minimal and the recovery after every cycle was the largest from all the investigated samples (Figure 5d). For I-x networks on the other hand, there was not a significant loss of strength compared to C-x but the deformation was still irreversible (Figure 5e) due to the dynamic nature of the ionic bonds. For this type of networks, the sliding and bending of the fibrils would be a more reasonable explanation for this deformation behavior.

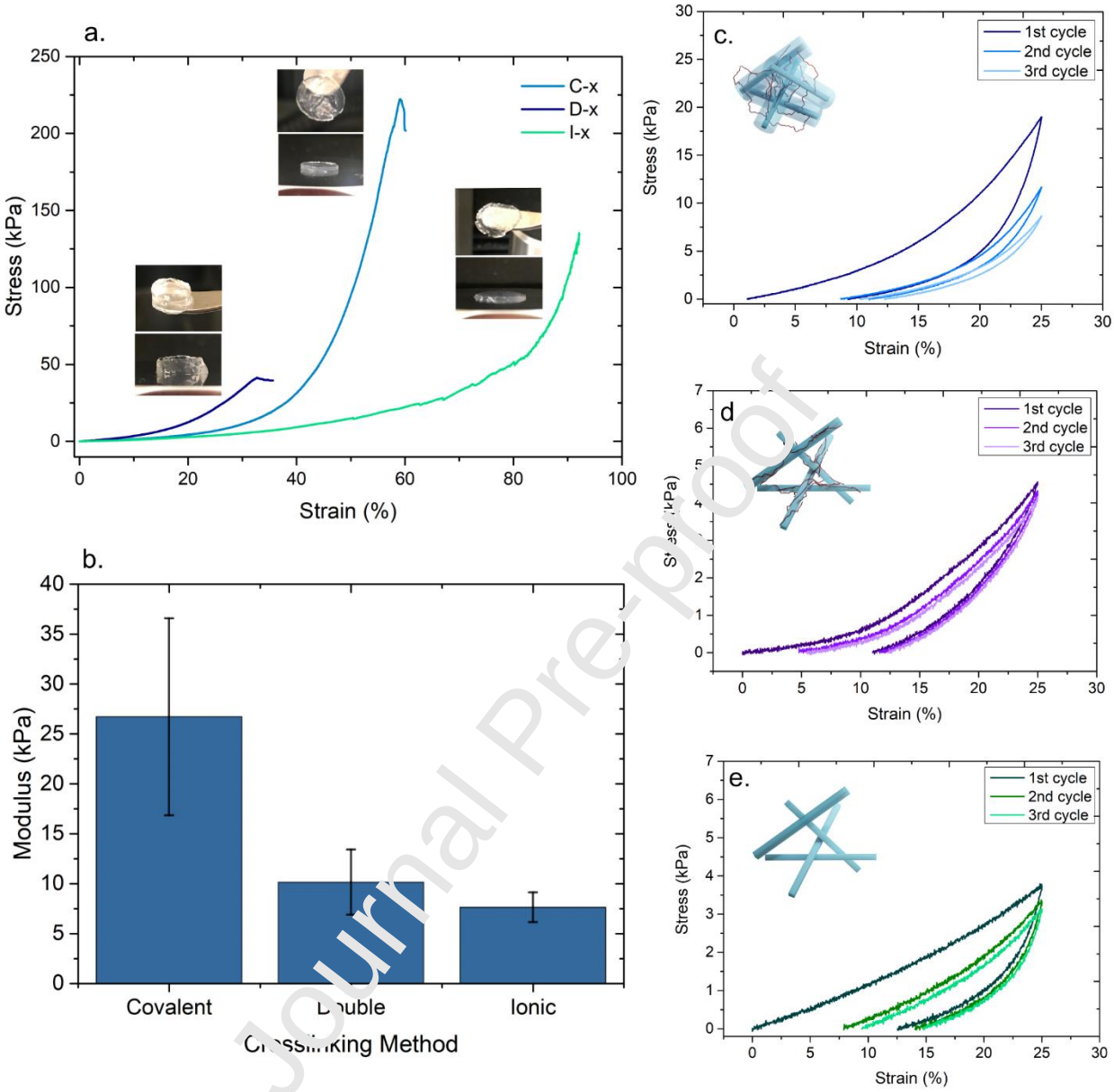

Fig. 5. *(a.) Compression loading profile and (b.) elastic modulus of the networks studied at an initial concentration of 1 wt.% CNF. First 3 compressive cycles of (c.) C-x, (d.) D-x and (e.) I-x networks at a 25% maximum strain*

3.5 Mathematical model that describes and predicts hydrogel behavior

While the physical bonds of the I-x networks slip under stress to modify/deform the network architecture, the more permanent nature of the bonds in the C-x networks, together with the compliance of the polymeric bridges between the fibrils, suggests that the C-x networks are more likely to behave nonlinear-elastically even at large deformations. To investigate this, a series of samples were soaked in solutions with concentrations of $CaCl_2$ ranging from 0 to

100mM. As expected, the degree of swelling of the samples was dependent on the concentration of salt, and it was observed from the compression-loading profiles that the strength and strain at break of the networks was indeed dependent on the swelling. Networks swollen in MilliQ water, which showed the highest degree of swelling, appeared brittle and weak compared to those with larger concentrations of salt. This behavior indicates that the internal pressure in the network plays an important role in the mechanism of deformation and failure of the network, as also discussed earlier.

Under uniaxial, compressive deformation, the network expands perpendicularly to the loading axis to distribute the load (Figure 6a). In a similar manner to the expansion due to swelling, this expansion due to uniaxial load requires the polymer bridges to stretch. In the case of highly swollen hydrogels, the polymer bridges holding the network together are already extended and the externally applied normal stress is inducing further stretching. This osmotic pre-stress is probably the cause of early breaking in the highly swollen networks.

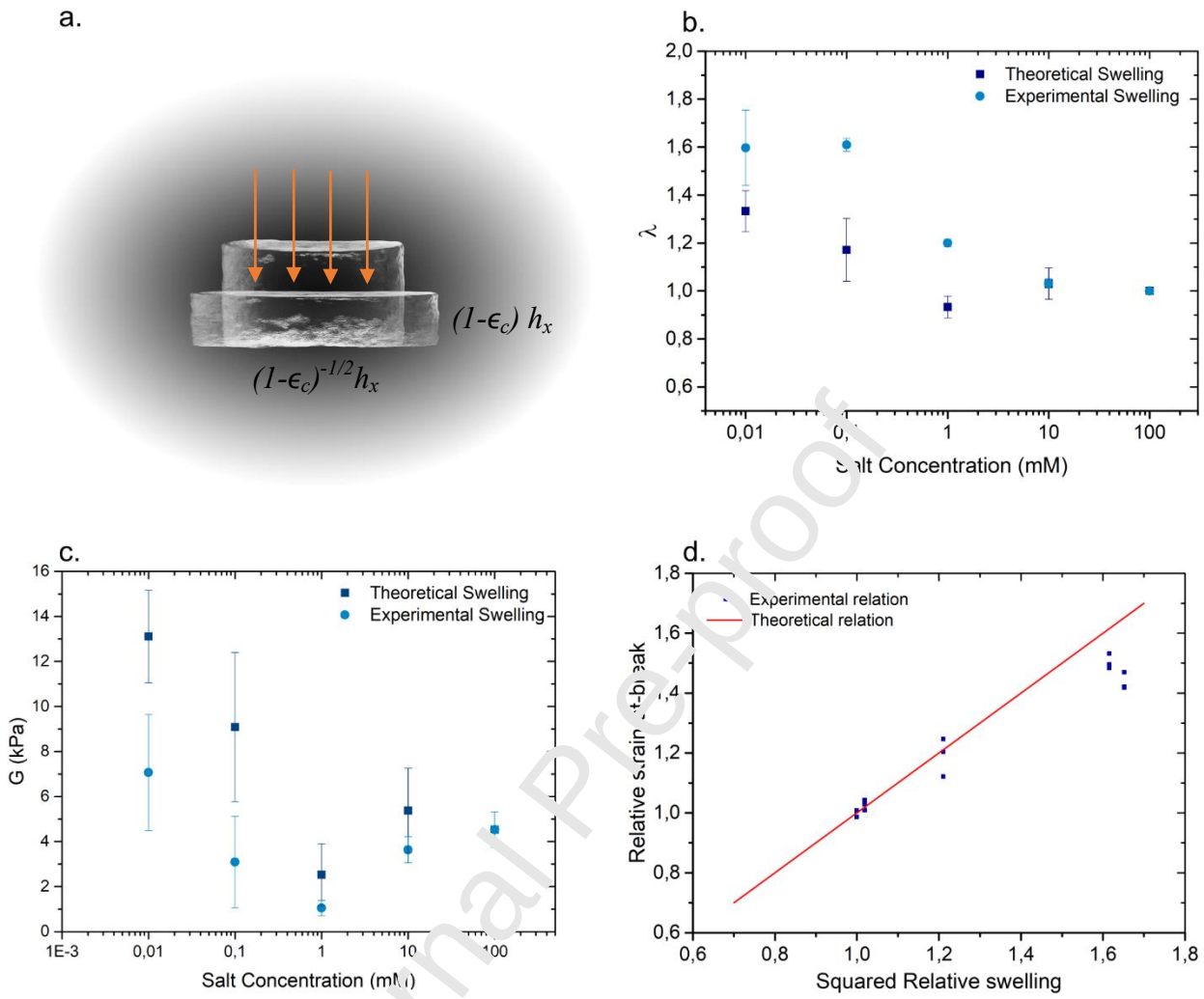

Fig. 6 *(a.) Schematic representation of the isochoric-deformation (constant volume) of the C-x hydrogel networks with width h_x before compression. (b.) Comparison between experimental swelling and model predictions (0.01mM represents swelling in MilliQ water). (c.). Shear modulus calculated from experimental swelling and predicted swelling (0.01mM represents swelling in MilliQ water). (d) Comparison of experimental and theoretical relations between strain at break and relative swelling.*

We propose to model this large-deformation constitutive behavior using the generalized neo-Hookean material model of Mooney and Rivlin(Mooney & H., 1940; Rivlin, 1948) (detailed model derivation in Supp. Info. II) which considers only the mechanical behavior of the network, while the effect of the solvent is modeled as added osmotic and hydrostatic contributions. During swelling, this network is in contact with an electrolyte reservoir, and osmotic and mixing pressures pre-stress the network at equilibrium to a stretch λ_s (swollen length divided by undeformed length). This reservoir is experimentally removed before the mechanical characterization. Thus, the osmotic pressure and the mixing pressure remain constant during deformation and such a deformation is isochoric, since no

discernable amount of solvent is expelled from the network during compression. The normal stress (normal force per undeformed area) applied to the network as a function of engineering compressive strain (ϵ_c) can then be obtained through straight-forward calculations (Supp. Info. II):

$$p_c(\epsilon_c) = \frac{6\lambda_s\epsilon_c\left(1-\epsilon_c+\frac{1}{3}\epsilon_c^2\right)[C_1(1-\epsilon_c)+C_2\lambda_s^2]}{(1-\epsilon_c)^3}, \quad (1)$$

and the shear modulus of the network becomes

$$G(\lambda_s) = \frac{2C_1}{\lambda_s} + 2C_2\lambda_s, \quad (2)$$

where C_1 and C_2 are material constants of the Mooney-Rivlin model. The absolute stretching of the network cannot be accessed experimentally. Therefore, λ_s is defined herein as the length ratio of the deformed to an approximately undeformed reference state. In order to fit the compressive data to Eq. (1), a reference state needs to be selected. Due to the presence of the surface charges on the fibrils, the network is pre-stressed even before it is crosslinked. Therefore, networks that were submerged in 100 mM $CaCl_2$, whose internal osmotic pressure was considered to be at its lowest degree, were selected as the reference state and assumed to have λ_s equal to 1. All other networks with larger swelling states would then have λ_s greater than 1.

The experimental data of the swelling stretch was obtained by weighing the as-prepared gel samples before and after they were soaked in $CaCl_2$ solutions at different concentrations and in Milli-Q water (See Supp Info. For more details). A relative swelling stretch λ_s^* with respect to the as-formed state was calculated as the cube root of the ratio between swollen gel weight and as-formed gel weight. Then, the proper swelling stretch λ_s of a sample was obtained as the ratio between λ_s^* for that sample and λ_s^* for the 100 mM salt sample.

The logarithm of the normal stress as a function of compressive strain was then plotted for all samples. Only data points up to 70% of the total stress at break where utilized since everything after this level would have signs of permanent failure where a more complex mechanism might be at play. The fitting of the data to the model was performed using two different strategies:

1. Assume that λ_s is equivalent to 1 for the least swollen networks, perform a fitting to the data to obtain values for the network parameters C_1 and C_2. Then use these constant values C_1 and C_2 and perform fitting

of λ_s to find a theoretical value for swelling stretch of swollen networks, which gives a predicted shear modulus at each state of swelling.

2. Utilize experimental data of the swelling of the network at different concentrations of salt solutions as parameter initiators and fit the network parameters C_1 and C_2 to the compressive stress-strain relation. Then, calculate the shear modulus using these parameters and the values from the experimental swelling.

The results from both approaches are observed in Figure 6b and 6c. It is clear from Figure 6 that regardless of whether the swelling stretch is fitted from the model or calculated from experimental outcomes, the qualitative trends in both swelling stretch and shear modulus are the same. Since the samples tested in the rheometer were prepared using a different procedure than those tested for compression, it is expected that the shear modulus G calculated from the model would only show semi-quantitative agreement with the rheological measurements. Comparison between these measurements should be performed with caution since they are aimed at obtaining different material properties at different length scales. Therefore, they cannot be compared directly in this work.

One source of error in the shear modulus originates from the idealized displacement field of the mechanical model, which assumes cylindrical symmetry; friction between the sample and the gritted disposable substrate breaks this symmetry in compression. This could be resolved by optimizing the experimental procedure reducing sample-substrate friction while prohibiting excessive lateral translation of the sample by some other constraint. This optimization, however, was out of scope of the current work. Another source of discrepancy is the relatively simple neo-Hookean material model with only two parameters. Generalized neo-Hookean models have the capability to describe details of large-deformation behavior (Ogden, 1997), and additional degrees of freedom in the model would give a better fit at both infinitesimal strains and large deformations, at the cost of introducing more material parameters.

Assuming also that the gel material fails when the network fails, a failure criterion was chosen based on the stretch of individual network strands. (Ayatollahi, Heydari-Meybodi, Dehghany, & Berto, 2016; Heydari-Meybodi, Ayatollahi, Dehghany, & Berto, 2017) The strands, whose stretch depends on both swelling and superposed deformation, are assumed to fail at a critical stretch λ_{cr}. In uniaxial compression, this stretch can be expressed as a

function of critical compressive strain at failure, ϵ_{cf}, as (the definition and derivation of this stretch is explained in Supp. Info. II)

$$\lambda_{cr} = \lambda_s \sqrt{\frac{1-\epsilon_{cf}+\epsilon_{cf}^2-\frac{1}{3}\epsilon_{cf}^3}{1-\epsilon_{cf}}} \quad (3)$$

The critical stretch λ_{cr} is assumed to be constant for a specific network architecture regardless of the swelling degree. Therefore, the swelling stretch for a network swollen to two different swelling states may be related to their respective strains-at-break as

$$\left(\frac{\lambda_{si}}{\lambda_{s0}}\right)^2 = \frac{\frac{1-\epsilon_{cf0}+\epsilon_{cf0}^2-\frac{1}{3}\epsilon_{cf0}^3}{1-\epsilon_{cf0}}}{\frac{1-\epsilon_{cfi}+\epsilon_{cfi}^2-\frac{1}{3}\epsilon_{cfi}^3}{1-\epsilon_{cfi}}}, \quad (4)$$

where 0 is a reference state and *i* represent different swollen states, respectively. If these assumptions hold true, equation 4 shows a linear relation between the squared relative swelling (left-hand side of Eq. (4)) and the relative strain-at-break (right-hand side of Eq. (4)) of the network. Figure 6d shows a comparison between the experimental results and the theoretical predictions for the relative strain-at-break as a function of the relative swelling of the C-x hydrogels having the least swollen of the samples as a reference for the relative swelling, i.e. hydrogels submerged in 100mM $CaCl_2$ prior to measurement. As shown in the figure, 6d, there is a good agreement between the experimental data and the theoretical predictions showing indeed that the assumptions on the effect of the relative swelling on the compressive strain-at-break of the hydrogels are sound.

It is then observed that, although the Mooney-Rivlin model underestimates the value of the swelling stretch and overestimates the shear modulus of the network, it is still a good fit for the experimental data. A possible explanation for the mismatch is the fact that the model does not account for the attractive interactions between the Ca^{2+} ions and the carboxylate groups on the surface of the fibrils, and thus, the possible creation of new ionic bonds as the network undergoes compressive deformation.

4 Conclusions

The differences in physical and mechanical properties of CNF networks crosslinked ionically and covalently were investigated in this work. We introduced a surface modification that enables the direct crosslinking of CNF networks utilizing poly-NIPAM as a flexible polymer linker. Our results indeed support the stated hypothesis where the presence of covalent crosslinks provided the network with improved physical and mechanical properties compared to ionically crosslinked by preventing sliding between the fibrils during deformation and/or water removal. However, close consideration must be given to the pre-loading stress due to swelling of the networks. The presence of a flexible linker provided the network with a rubber-like elasticity and the mechanical properties of the resulting network could be tuned through changes of ionic strength and volume fraction of cellulose. These hydrogels also exhibit an extraordinary shape recovery and reswelling capacity across drying cycles at weight fractions as low as 2 wt.% which was not observed for hydrogels crosslinked with divalent salt ($CaCl_2$). The properties of the networks as well as the polymerization were extensively characterized using X-ray scattering, rheology and compression loading. The structures of the networks and their deformation mechanisms were analyzed and compared for the different crosslinking methods. Furthermore, a mathematical model that estimates the mechanical behavior and the swelling of the C-x hydrogels was developed based on experimental observations. This semi-quantitative model relates the macroscopic behavior to the internal phenomena in the networks, and corroborates our hypothesis that the swelling pre-stress acts to embrittle the hydrogel.

Conflicts of Interest

There are no conflicts to declare.

Acknowledgements

This work was supported by the Knut and Alice Wallenberg foundation through the Wallenberg Wood Science Center and of the Royal Swedish Academy of Agriculture and Forestry via Tandem Forest Values research program (TFV 2018-0029). SBL works within the research profile Neopulp financed by the Knowledge foundation. SBL thanks Svenska Cellulosa AB (SCA) for financial support. The authors also would like to acknowledge Dr. Xiaoju Wang, Professor Tomas Larsson, Dr. Tobias Benselfelt, Dr. Johan Erlandsson and Dr. Jonas Garemark for the fruitful discussions and guidance. Furthermore, thanks to Anita Teleman and Treesearch Infrastructure for their funding and support.

Data Availability

Data will be available upon request

References

Apelgren, P., Amoroso, M., Saljo, K., Lindahl, A., Brantsing, C., Stridh Orrhult, L., . . . Kolby, L. (2021). Long-term in vivo integrity and safety of 3D-bioprinted cartilaginous constructs. *J Biomed Mater Res B Appl Biomater,* 109(1), 126-136.

Ashammakhi, N., Ahadian, S., Xu, C., Montazerian, H., Ko, H., Nasiri, R., . . . Khademhosseini, A. (2019). Bioinks and bioprinting technologies to make heterogeneous and biomimetic tissue constructs. *Mater Today Bio,* 1, 100008.

Aulin, C., Johansson, E., Wågberg, L., & Lindström, T. (2010). Self-Organized Films from Cellulose I Nanofibrils Using the Layer-by-Layer Technique. *Biomacromolecules,* 11(4), 872-882.

Ayatollahi, M. R., Heydari-Meybodi, M., Dehghany, M., & Berto, F. (2016). A New Criterion for Rupture Assessment of Rubber-Like Materials under Mode-I Crack Loading: The Effective Stretch Criterion. *Advanced Engineering Materials,* 18(8), 1364-1370.

Benselfelt, T., Nordenström, M., Hamedi, M. M., & Wågberg, L. (2019). Ion-induced assemblies of highly anisotropic nanoparticles are governed by ion–ion correlation and specific ion effects. *Nanoscale,* 11(8), 3514-3520.

Benselfelt, T., Nordenström, M., Lindström, S. B., & Wågberg, L. (2019). Explaining the Exceptional Wet Integrity of Transparent Cellulose Nanofibril Films in the Presence of Multivalent Ions—Suitable Substrates for Biointerfaces. *Advanced Materials Interfaces,* 6(13).

Bratko, D., Jönsson, B., & Wennerström, H. (1986). Electrical double layer interactions with image charges. *Chemical Physics Letters,* 128(5), 449-454.

Creton, C. (2017). 50th Anniversary Perspective: Networks and Gels: Soft but Dynamic and Tough. *Macromolecules,* 50(21), 8297-8316.

Foster, E. J., Moon, R. J., Agarwal, U. P., Bortner, M. J., Bras, J., Camarero-Espinosa, S., . . . Youngblood, J. (2018). Current characterization methods for cellulose nanomaterials. *Chemical Society Reviews,* 47(8), 2609-2679.

Hagiwara, Y., Putra, A., Kakugo, A., Furukawa, H., & Gong, J. P. (2009). Ligament-like tough double-network hydrogel based on bacterial cellulose. *Cellulose,* 17(1), 93-101.

Heise, K., Kontturi, E., Allahverdiyeva, Y., Tammelin, T., Linder, M. B., Nonappa, & Ikkala, O. (2021). Nanocellulose: Recent Fundamental Advances and Emerging Biological and Biomimicking Applications. *Advanced Materials,* 33(3), 2004349.

Heydari-Meybodi, M., Ayatollahi, M. R., Dehghany, M., & Berto, F. (2017). Mixed-mode (I/II) failure assessment of rubber materials using the effective stretch criterion. *Theoretical and Applied Fracture Mechanics,* 91, 126-133.

Hill, R. J. (2008). Elastic modulus of microfibrillar cellulose gels. *Biomacromolecules,* 9(10), 2963-2966.

Isogai, A., Saito, T., & Fukuzumi, H. (2011). TEMPO-oxidized cellulose nanofibers. *Nanoscale,* 3(1), 71-85.

Kang, H., Liu, R., & Huang, Y. (2016). Cellulose-Based Gels. *Macromolecular Chemistry and Physics,* 217(12), 1322-1334.

Kelly, P. V., Cheng, P., Gardner, D. J., & Gramlich, W. M. (2021). Aqueous Polymer Modification of Cellulose Nanofibrils by Grafting-Through a Reactive Methacrylate Group. *Macromol Rapid Commun,* 42(3), e2000531.

Laivins, G., & Scallan, A. (1993). The mechanism of hornification of wood pulps. *Products of papermaking,* 2, 1235.

Lee, Y., Song, W. J., & Sun, J. Y. (2020). Hydrogel soft robotics. *Materials Today Physics,* 15.

Markstedt, K., Escalante, A., Toriz, G., & Gatenholm, P. (2017). Biomimetic Inks Based on Cellulose Nanofibrils and Cross-Linkable Xylans for 3D Printing. *ACS Appl Mater Interfaces,* 9(46), 40878-40886.

Markstedt, K., Mantas, A., Tournier, I., Martinez Avila, H., Hagg, D., & Gatenholm, P. (2015). 3D Bioprinting Human Chondrocytes with Nanocellulose-Alginate Bioink for Cartilage Tissue Engineering Applications. *Biomacromolecules,* 16(5), 1489-1496.

Mayumi, K., Guo, J., Narita, T., Hui, C. Y., & Creton, C. (2016). Fracture of dual crosslink gels with permanent and transient crosslinks. *Extreme Mechanics Letters,* 6, 52-59.

Michalik, R., & Wandzik, I. (2020). A Mini-Review on Chitosan-Based Hydrogels with Potential for Sustainable Agricultural Applications. *Polymers (Basel),* 12(10).

Mooney, M., & H., H. (1940). A Theory of Large Elastic Deformation. *Journal of Applied Physics,* 11(9), 582-592.

Nechyporchuk, O., Belgacem, M. N., & Bras, J. (2016). Production of cellulose nanofibrils: A review of recent advances. *Industrial Crops and Products,* 93, 2-25.

Nemir, S., & West, J. L. (2010). Synthetic materials in the study of cell response to substrate rigidity. *Ann Biomed Eng,* 38(1), 2-20.

Ng, H.-M., Sin, L. T., Bee, S.-T., Tee, T. T., & Rahmat, A. R. (2017). Review of Nanocellulose Polymer Composite Characteristics and Challenges. *Polymer-Plastics Technology and Engineering,* 56(7), 687-731.

Ogden, R. W. (1997). *Non-linear elastic deformations*: Courier Corporation.

Pääkkö, M., Ankerfors, M., Kosonen, H., Nykänen, A., Ahola, S., Österberg, M., . . . Lindström, T. (2007). Enzymatic Hydrolysis Combined with Mechanical Shearing and High-Pressure Homogenization for Nanoscale Cellulose Fibrils and Strong Gels. *Biomacromolecules,* 8(6), 1934-1941.

Peng, N., Huang, D., Gong, C., Wang, Y., Zhou, J., & Chang, C. (2020). Controlled Arrangement of Nanocellulose in Polymeric Matrix: From Reinforcement to Functionality. *ACS Nano,* 14(12), 16169-16179.

Qiao, L., Du, C., Gong, J. P., Wu, Z. L., & Zheng, Q. (2019). Programmed Diffusion Induces Anisotropic Superstructures in Hydrogels with High Mechano- Optical Sensitivity. *Advanced Materials Technologies,* 4(11).

Rivlin, R. S. (1948). Large elastic deformations of isotropic materials IV. Further developments of the general theory. *Philosophical transactions of the royal society of London. Series A, Mathematical and physical sciences,* 241(835), 379-397.

Rol, F., Belgacem, M. N., Gandini, A., & Bras, J. (2019). Recent advances in surface-modified cellulose nanofibrils. *Progress in Polymer Science,* 88, 241-264.

Rudzinski, W. E., Dave, A. M., Vaishnav, U. H., Kumbar, S. G., Kulkarni, A. R., & Aminabhavi, T. M. (2012). Hydrogels as controlled release devices in agriculture. *Designed Monomers and Polymers,* 5(1), 39-65.

Sachyani Keneth, E., Kamyshny, A., Totaro, M., Beccai, L., & Magdassi, S. (2021). 3D Printing Materials for Soft Robotics. *Adv Mater,* 33(19), e2003387.

Saito, T., Hirota, M., Tamura, N., Kimura, S., Fukuzumi, H., Heux, L., & Isogai, A. (2009). Individualization of nano-sized plant cellulose fibrils by direct surface carboxylation using TEMPO catalyst under neutral conditions. *Biomacromolecules,* 10(7), 1992-1996.

Saito, T., Uematsu, T., Kimura, S., Enomae, T., & Isogai, A. (2011). Self-aligned integration of native cellulose nanofibrils towards producing diverse bulk materials. *Soft Matter,* 7(19).

Shiblee, M. D. N. I., Ahmed, K., Kawakami, M., & Furukawa, H. (2019). 4D Printing of Shape-Memory Hydrogels for Soft- Robotic Functions. *Advanced Materials Technologies,* 4(8).

Tatsumi, D., Inaba, D., & Matsumoto, T. (2008). Layered structure and viscoelastic properties of wet pulp fiber networks. *Nihon Reoroji Gakkaishi,* 36(5), 235-239.

Tatsumi, D., Ishioka, S., & Matsumoto, T. (2002). Effect of fiber concentration and axial ratio on the rheological properties of cellulose fiber suspensions. *Nihon Reoroji Gakkaishi,* 30(1), 27-32.

Wågberg, L., Decher, G., Norgren, M., Lindström, T., Ankerfors, M., & Axnäs, K. (2008). The Build-Up of Polyelectrolyte Multilayers of Microfibrillated Cellulose and Cationic Polyelectrolytes. *Langmuir,* 24(3), 784-795.

Wang, Q., Backman, O., Nuopponen, M., Xu, C., & Wang, X. (2021). Rheological and Printability Assessments on Biomaterial Inks of Nanocellulose/Photo-Crosslinkable Biopolymer in Light-Aided 3D Printing. *Frontiers in Chemical Engineering,* 3.

Wang, X., Wang, Q., & Xu, C. (2020). Nanocellulose-Based Inks for 3D Bioprinting: Key Aspects in Research Development and Challenging Perspectives in Applications-A Mini Review. *Bioengineering (Basel),* 7(2).

Xu, W., Molino, B. Z., Cheng, F., Molino, P. J., Yue, Z., Su, D., . . . Wallace, G. G. (2019). On Low-Concentration Inks Formulated by Nanocellulose Assisted with Gelatin Methacrylate (GelMA) for 3D Printing toward Wound Healing Application. *ACS Appl Mater Interfaces,* 11(9), 8838-8848.

Xu, W., Zhang, X., Yang, P., Langvik, O., Wang, X., Zhang, Y., . . . Xu, C. (2019). Surface Engineered Biomimetic Inks Based on UV Cross-Linkable Wood Biopolymers for 3D Printing. *ACS Appl Mater Interfaces,* 11(13), 12389-12400.

Yanase, K., Buchner, R., & Sato, T. (2018). Microglobule formation and a microscopic order parameter monitoring the phase transition of aqueous poly(N-isopropylacrylamide) solution. *Physical Review Materials,* 2(8), 085601.

Zinge, C., & Kandasubramanian, B. (2020). Nanocellulose based biodegradable polymers. *European Polymer Journal,* 133, 109758.

Author Contributions

Maria F. Cortes Ruiz- Methodology, Validation, Formal analysis, Investigation, Data curation, Visualization, Writing - original draft, review and editing.

Yury Brusentsev- Methodology, Formal analysis, Data curation, Writing – original draft review and editing.

Stefan B. Lindström- Methodology, Software, Formal analysis, Writing –original draft, review and editing, Visualization

Chunlin Xu- Methodology, Writing- review and editing,

Lars Wågberg- Conceptualization, Methodology, Resources, Supervision, Writing- review and editing, Project administration and Funding acquisition.

Declaration of interests

☒The authors declare that they have no known competing financial interests or personal relationships that could have appeared to influence the work reported in this paper.

☐The authors declare the following financial interests/personal relationships which may be considered as potential competing interests:

Graphical abstract